Mirrored one-nucleon knockout reactions to the $T_z = \pm\frac{3}{2}$ A=53 mirror nuclei

S. A. Milne,[1] M. A. Bentley,[1] E. C. Simpson,[2] P. Dodsworth,[1] T. Baugher,[3,4] D. Bazin,[4] J. S. Berryman,[4] A. M. Bruce,[5] P. J. Davies,[1] C. Aa. Diget,[1] A. Gade,[3,4] T. W. Henry,[1] H. Iwasaki,[3,4] A. Lemasson,[4,6] S. M. Lenzi,[7] S. McDaniel,[3,4] D. R. Napoli,[8] A. J. Nichols,[1] A. Ratkiewicz,[3,4] L. Scruton,[1] S. R. Stroberg,[3,4] J. A. Tostevin,[9] D. Weisshaar,[4] K. Wimmer,[4,10] and R. Winkler[4]

[1]*Department of Physics, University of York, Heslington, York YO10 5DD, United Kingdom*
[2]*Department of Nuclear Physics, Research School of Physics and Engineering, Australian National University, Canberra, Australian Capital Territory 2601, Australia*
[3]*Department of Physics and Astronomy, Michigan State University, East Lansing, Michigan 48824, USA*
[4]*National Superconducting Cyclotron Laboratory, Michigan State University, East Lansing, Michigan 48824, USA*
[5]*School of Computing, Engineering and Mathematics, University of Brighton, Brighton BN2 4GJ, United Kingdom*
[6]*GANIL, CEA/DSM-CNRS/IN2P3, BP55027, F-14076, Caen Cedex 5, France*
[7]*Dipartimento di Fisica del'Universita and INFN, Sezione di Padova, I-35131 Padova, Italy*
[8]*INFN, Laboratori Nazionali di Legnaro, I-35020 Legnaro, Italy*
[9]*Department of Physics, Faculty of Engineering and Physical Sciences, University of Surrey, Guildford GU2 7XH, United Kingdom and*
[10]*Department of Physics, The University of Tokyo, 7-3-1 Hongo, Bunkyo-ku, TOKYO 113-0033 Japan*

(Dated: February 3, 2016)

Background: The study of excited states in mirror nuclei allows us to extract information on charge-dependent (i.e. isospin-non-conserving) interactions in nuclei.

Purpose: To extend previous studies of mirror nuclei in the $f_{\frac{7}{2}}$ region, investigating charge symmetry breaking (CSB) of the strong nuclear force.

Methods: Gamma-ray spectroscopy has been performed for the mirror ($T_z = \pm\frac{3}{2}$) pair ^{53}Ni and ^{53}Mn, produced via mirrored one-nucleon knockout reactions.

Results: Several new transitions have been identified in ^{53}Ni from which a new level scheme has been constructed. Cross sections for knockout have been analysed and compared with reaction model calculations where evidence is found for knockout from high-spin isomeric states. Mirror energy differences (MED) between isobaric analogue states (IAS) have been computed, compared to large scale shell-model calculations and interpreted in terms of isospin non-conserving effects. In addition, lifetimes for the long-lived $J^\pi = \frac{5}{2}^-_1$ analogue states in both ^{53}Mn and ^{53}Ni have been extracted through lineshape analysis, giving half-lives of $t_{\frac{1}{2}} = 120(14)$ ps and $t_{\frac{1}{2}} = 198(12)$ ps, respectively.

Conclusions: The inclusion of a set of isovector isospin-non-conserving matrix elements to the shell-model calculations gave the best agreement with the experimental data.

I. INTRODUCTION

In the absence of the electromagnetic interaction, the proton and neutron can be considered as two quantum states of the same particle, the nucleon. In order to distinguish between these particles, they are assigned an isospin quantum number $t = \frac{1}{2}$ with a projection t_z along an isospin quantization axis. In this construct the proton is assigned a projection $t_z = -\frac{1}{2}$ and the neutron $t_z = +\frac{1}{2}$, whereby the total isospin projection of the nucleus is given by the sum of the individual isospin projections, $T_z = (N - Z)/2$ [1]. This concept is also dependent upon the strong nuclear force being charge independent and charge symmetric, and indeed experiment has shown the nucleon-nucleon interactions to be approximately equal for neutron-neutron, proton-proton and neutron-proton pairs [2]. In the absence of isospin-breaking interactions, one would expect degeneracy between analogue states in nuclei of the same mass number [Isobaric Analogue States (IAS)]. Differences in excitation energy of IAS will result from isospin-breaking effects such as Coulomb and magnetic effects and any charge dependence of the nucleon-nucleon interaction. The differences between excitation energies of IAS in mirror nuclei are known as Mirror Energy Differences (MED), defined as follows:

$$MED_J = E^*_{J,T,-T_z} - E^*_{J,T,T_z} \quad (1)$$

where E^*_{J,T,T_z} represents the excitation energy of a state of spin, J, isospin, T and isospin projection, T_z.

Recent work in the $f_{\frac{7}{2}}$ region, focusing mainly on mirror nuclei, has resulted in the development of a detailed description of MED in terms of these isospin-breaking phenomena – see for example references [3–7]. This work has shown the need for the inclusion, in the shell-model prescription, of an additional isovector term that behaves like a spin-dependent, charge-symmetry-breaking (CSB) term to better reproduce the experimental data [3, 4, 6, 7]. The origin of this phenomenon is still unclear, and has usually been accounted for in the

model by adding a single repulsive interaction of 100 keV (in addition to the Coulomb interaction) to the two-body matrix elements for $f_{\frac{7}{2}}$ protons coupled to $J = 2$ [4, 6]. The motivation for this work was to extend on previous studies in the region and to study excited states in mirror nuclei at large isospin, in this case the $T = \frac{3}{2}$ ($T_z = \pm\frac{3}{2}$) pair ^{53}Ni and ^{53}Mn.

In this work, we present new data on excited states in the proton-rich $T_z = -\frac{3}{2}$ system ^{53}Ni and its mirror ^{53}Mn. States in ^{53}Ni have only been tentatively reported in one previous experiment, in which ^{53}Ni and ^{53}Mn were populated via -3n and -3p removal/fragmentation reactions from a ^{56}Ni secondary beam at the National Superconducting Cyclotron Laboratory (NSCL) at Michigan State University (MSU) [8]. Due to low statistics, only two transitions could be identified in ^{53}Ni, at $\sim$320 keV and 1453 keV, believed to correspond to the $J^\pi{:}\frac{5}{2}_1^- \rightarrow \frac{7}{2}^-_{g.s}$ and $J^\pi{:}\frac{11}{2}_1^- \rightarrow \frac{7}{2}^-_{g.s}$ transitions, respectively. However, due to its expected long half-life, the excitation energy and half-life of the the $(\frac{5}{2}_1^-)$ state could not be accurately measured. The more neutron-rich mirror ^{53}Mn, however, has a well-known level scheme identified in previous experiments [9–11]. This includes a half-life measurement of the long-lived $\frac{5}{2}_1^-$ state, with a measured half-life of $T_{\frac{1}{2}} = 117(6)$ ps [11].

This work also investigates the use of knockout reactions to populate excited states in exotic proton-rich nuclei and their mirrors in this region [3, 8, 12]. In terms of direct reactions, mirrored two-nucleon knockout reactions have recently been employed in the study of $T = 2$ mirror nuclei [8]. In this work, we present a study of a mirror pair using "mirrored" one-nucleon knockout reactions. The direct nature of the population of states in these mirror nuclei, coupled to the isospin symmetric reactions employed, allows significant confidence in the assignment of the states in the exotic ^{53}Ni nucleus. The present study also allows for a stringent test of the nuclear shell model effective interactions in this region, particularly through MED and cross-section measurements.

II. EXPERIMENTAL DETAILS

The experiment was performed at the National Superconducting Cyclotron Laboratory (NSCL) at Michigan State University (MSU), where excited states in the mirror nuclei ^{53}Ni ($T_z = -\frac{3}{2}$) and ^{53}Mn ($T_z = +\frac{3}{2}$) were populated via one-neutron and one-proton knockout, respectively, from the secondary beams of ^{54}Ni ($T_z = -1$) and ^{54}Fe ($T_z = +1$) - which are themselves a mirror pair. Due to the symmetry of the reactions (which we refer to as "mirrored knockout") used to populate these nuclei and therefore their respective excited states, the γ-ray spectra (produced under identical conditions) can be used to identify mirror transitions. This therefore gives high confidence to the spin and parity assignments made using mirror symmetry arguments, when the analogue states are both particle bound. This new approach to MED studies has already shown great potential in previous work studying proton-rich nuclei in this region [3, 8, 12].

The secondary beams of interest, ^{54}Ni and ^{54}Fe, were produced via the fragmentation of a 160 MeV/nucleon ^{58}Ni primary beam impinging upon a 802 mg/cm^2 ^{9}Be production target, positioned at the entrance of the A1900 separator. The resulting fragments were separated by the A1900 [13, 14], before being transferred to the S800 spectrograph. These secondary beam fragments were then identified from their time-of-flight (ToF) measured between two plastic scintillators located in the A1900 fragment separator and the object position of the S800 beam line, respectively. At the secondary target position, in the S800 spectrograph [15, 16], a ^{9}Be reaction target of areal density 188 mg/cm^2 was used to populate excited states in the nuclei of interest via mirrored one-nucleon knockout reactions from the $\sim$87 MeV/nucleon ^{54}Ni and ^{54}Fe secondary beams. In-flight γ-ray decays of the reaction residues were detected by the Segmented Germanium Array (SeGA) detectors [17], positioned in two rings at 37° and 90°, with respect to the beam axis. Particle identification was achieved through measuring the energy loss in the S800 ionization chamber and the time-of-flight through the S800 spectrograph. The γ-rays detected by the SeGA detectors were associated with the correct fragments through coincidence conditions.

III. RESULTS

The Doppler corrected γ-ray spectra for ^{53}Mn and ^{53}Ni, populated via one-nucleon knockout from ^{54}Fe and ^{54}Ni, respectively, are presented in Fig. 1(a) and (b). A comparison of the spectra demonstrates a clear one-to-one correspondence between the strongest γ-ray peaks observed. However, for some of the weaker transitions, the correspondence is less clear, but some suggestions for this are presented later. Through careful analysis, involving both the use of spectral comparison and, more importantly, γ-γ coincidence analysis, a new level scheme for ^{53}Ni was deduced, as shown in Fig. 2. The ordering of the transitions has been confirmed by both γ-γ coincidence analysis and transition intensities. The spins and parities have been assigned on mirror symmetry arguments. Whilst the direct, mirrored, reaction process gives confidence in the spin/parity assignments presented, they have not been formally measured and so they are presented here in parentheses. The two transitions previously reported by Brown *et al.* [8], assigned to decays from the yrast $\frac{5}{2}^-$ and $\frac{11}{2}^-$ states, are confirmed here. In the previous work [8] the energy of the γ-decay from the $(\frac{5}{2}_1^-)$ state could not be accurately measured, due to its long half-life, but has now been established as 320(3) keV from the energy difference between the 972 keV and 1292 keV prompt γ-ray transitions.

A detailed understanding of which of the known states

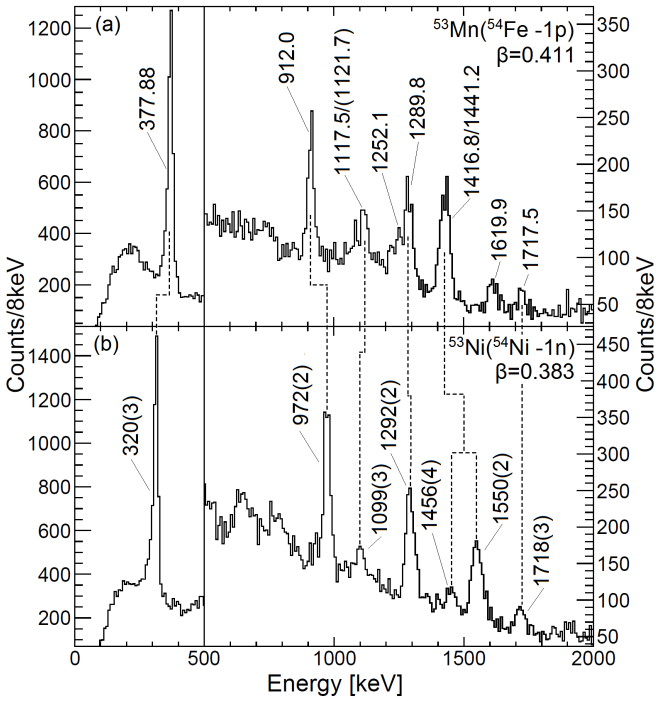

FIG. 1. The Doppler corrected spectra for γ-rays in coincidence with the (a) ^{53}Mn and (b) ^{53}Ni fragments, where β was optimised to give the best resolution for the fast transitions. The dashed lines indicate the proposed analogue transitions in the mirror nuclei. Transition energy labels for ^{53}Mn are shown from more accurate previous measurements [10].

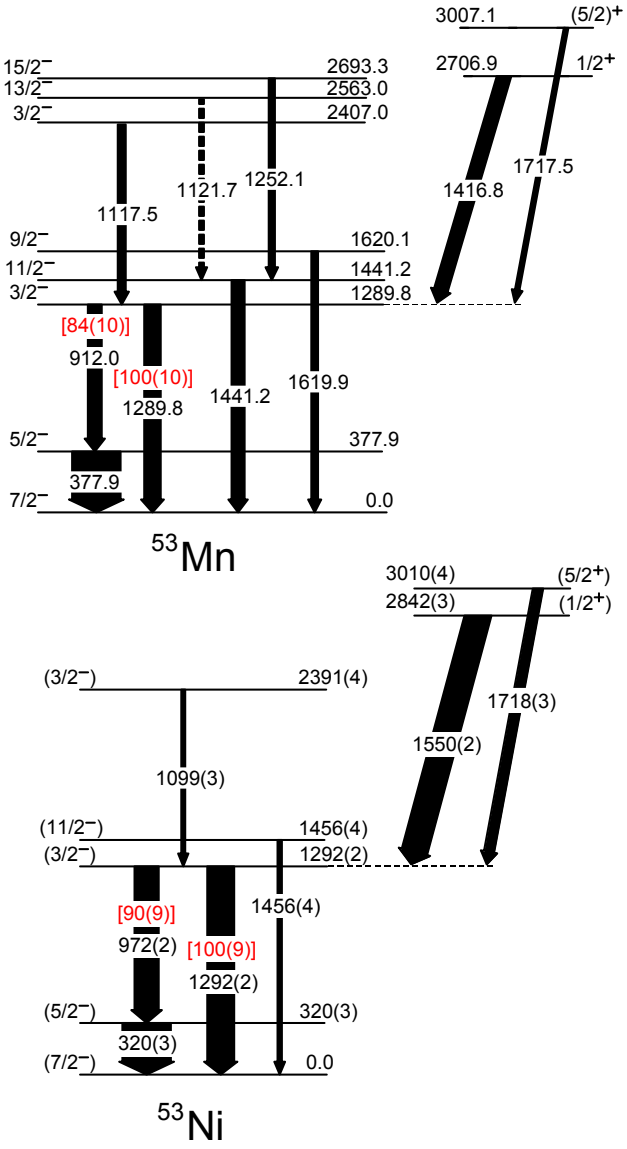

FIG. 2. (color online). The energy level schemes for ^{53}Ni and ^{53}Mn as observed in this work. The spins and parities are in parentheses for ^{53}Ni as the assignments are made on mirror-symmetry arguments. Tentative transitions are indicated by dashed lines. Branching ratios for the $\frac{3}{2}^-_1$ level are indicated in red with square brackets and the energy labels used for ^{53}Mn come from more accurate previous measurements [10]. The widths of the arrows are proportional to the relative γ-ray intensities observed.

in ^{53}Mn are being populated, and the mechanism through which this occurs, is essential in order to help establish the new scheme of ^{53}Ni, populated through the analogue knockout process. A partial level scheme of ^{53}Mn, using information from [10], is also shown in Fig. 2. Only the transitions observed in this work are shown. One of the states in question, the known $\frac{13}{2}^-$ state, is only said to be tentatively observed. This is because the transition we observe has a measured energy of 1118(4) keV and is likely to correspond to the 1117.5 keV transition from the $(\frac{3}{2}^-_2)$ state, with a possible contribution from the 1121.7 keV transition from the $\frac{13}{2}^-$ state. It will be shown later that the mechanism that populates the $\frac{15}{2}^-$ state (which is observed) is also expected to populate the $\frac{13}{2}^-$ state. Furthermore, the observed transition has a significantly larger relative intensity than the mirror transition in ^{53}Ni and therefore may be a 1117.5/1121.7 doublet.

Knockout reactions from ^{54}Ni (^{54}Fe) are expected to populate negative-parity states with $J^\pi = \frac{7}{2}^-$, $\frac{3}{2}^-$, $\frac{5}{2}^-$ and $\frac{1}{2}^-$ through removal of $f_{\frac{7}{2}}$, $p_{\frac{3}{2}}$, $f_{\frac{5}{2}}$ and $p_{\frac{1}{2}}$ neutrons (protons) near the Fermi level. Being below ^{56}Ni, the spectroscopic strength to the $\frac{1}{2}^-$, $\frac{3}{2}^-$ and $\frac{5}{2}^-$ states is expected to be weak and, moreover, measured spectroscopic factors for proton removal from ^{54}Fe to ^{53}Mn [18] indicate that the bulk of the $f_{\frac{7}{2}}$ spectroscopic strength lies in the $J^\pi = \frac{7}{2}^-$ ground state. Thus, we expect direct population of all the negative parity excited states in ^{53}Ni and ^{53}Mn to be weak. This is verified in Fig. 2, where it is seen that a significant amount of the intensity observed proceeding through excited states in these mirror nuclei comes from direct population of positive-parity states with $J^\pi = (\frac{5}{2})^+$ and $\frac{1}{2}^+$, through removal of $d_{(\frac{5}{2})}$ and $s_{\frac{1}{2}}$ neutrons(protons) from ^{54}Ni(^{54}Fe). In addi-

tion to these hole states, there is evidence for higher-spin negative-parity states being populated in both nuclei. For example, $J^\pi = \frac{11}{2}^-$ states are observed in both nuclei, which cannot be populated by a direct reaction from the ground state of the beam. In addition, higher-spin states are observed more strongly in ^{53}Mn. These data indicate the presence of isomeric state(s) in the beam(s) and will be discussed later.

The spin assignment of the 3007.1-keV [10] positive-parity state in ^{53}Mn, $J^\pi = (\frac{5}{2})^+$ in Fig. 2, is uncertain. Its first observation in a proton-stripping reaction was shown to correspond to $l = 2$ [19]. From this, it was assumed to correspond to removal of a $d_{\frac{3}{2}}$ proton from ^{54}Fe, and thus the state would have an assignment of $\frac{3}{2}^+$. Subsequent papers have since used this assignment. However, the current evaluated nuclear data compilation [10] has this state as a tentative $\frac{5}{2}^+$, based on the observed direct decay to the ground state, assumed to be a dipole transition. Earlier work [20] has demonstrated, through energy centroid shift methods, that this state has a half-life lower limit of 0.84 ps. In order to gain some further information on this half-life, and to help resolve this assignment, we have performed a Doppler correction analysis, whereby the optimum β-value to align a γ-ray peak in both the 37° and 90° SeGA rings, is determined. This analysis has shown that a β-value of ∼0.41 is required for the other fast transitions in ^{53}Mn with half-lives ∼1 ps. These transitions are emitted with the largest value of β as they are emitted from within the target volume. It takes around 8 ps for the beam to traverse the target thickness and therefore for states with half-lives of the order of 10 ps and greater, the majority of decays take place downstream of the target, where the emitter velocity has been reduced due to energy loss in the target. For example, we find a β-value of 0.390(2) is required to align the γ-rays associated with the decay of the long-lived $J^\pi = \frac{5}{2}^-_1$ state, which is known to decay downstream of the target. These numbers are consistent with LISE++ [21] calculations that predict a change in β from the center (i.e. the average interaction point) to the back of the target from 0.409 to 0.394. Our analysis for the 1717.5-keV transition yielded a β-value of 0.416(6), where the error comes from our estimate of the uncertainty in aligning the transition energies in the two detector rings. Thus, our experimental data clearly point to the average point of decay being inside the target volume, and so we can put a safe upper limit on the half-life of ∼4 ps. The 3007.1-keV state is known to decay to the $\frac{7}{2}^-$ ground state with a 14% branch [22] and depending on whether it has a spin of $\frac{3}{2}$ or $\frac{5}{2}$ will determine whether it decays via an M2 or E1 transition. Typical transition strengths for M2 transitions in the A=45-90 region have been observed in the range of 0.02→0.2 W.u. whilst E1 transitions have typically been observed in the range of $(10^{-6}\rightarrow10^{-4})$ W.u. [23]. With a maximum 4 ps half-life for the 3007.1-keV state, the M2 and E1 transition strengths would be a minimum of 0.3 W.u. and 6×10^{-7} W.u., respectively. This lower-limit M2 transition strength is above the typical range, but nevertheless below the recommended upper limit of 1 W.u. proposed in reference [23]. Thus, we cannot make a firm assignment here, although the systematics suggest that the current assignment of $\frac{5}{2}^+$ is more likely. We have assumed this tentative assignment in the following analysis, although the conclusions do not depend strongly on this assumption.

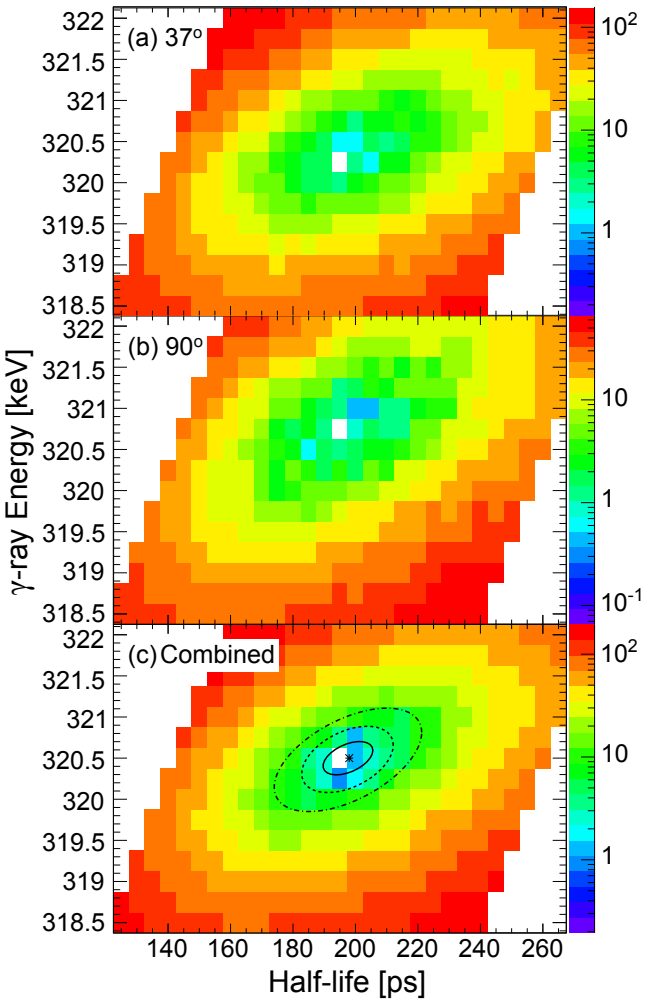

FIG. 3. (color online). Plot of $\chi^2-\chi^2_{min}$ for simulated spectra (varying either energy or half-life) fitted to the ^{53}Ni experimental spectra for the J^π:$(\frac{5}{2}^-_1)\rightarrow(\frac{7}{2}^-_{g.s})$ transition in (a) the 37° SeGA ring and (b) the 90° SeGA ring. (c) The combined $\chi^2-\chi^2_{min}$ plot of (a) and (b) where the χ^2_{min} point corresponds to 320.5 keV and 198 ps. Statistical errors in (c) are shown by ellipses, whereby the $\pm1\sigma$, $\pm2\sigma$ and $\pm3\sigma$ errors are represented by a solid line, a dashed line and a dash-dot line respectively. See text for more details.

Due to the long half-life (117(6) ps [11]) of the $\frac{5}{2}^-_1$ state in ^{53}Mn (and presumably in ^{53}Ni), decays from this state occur up to a few cm downstream of the target. This has the effect of smearing the effective angle for the SeGA de-

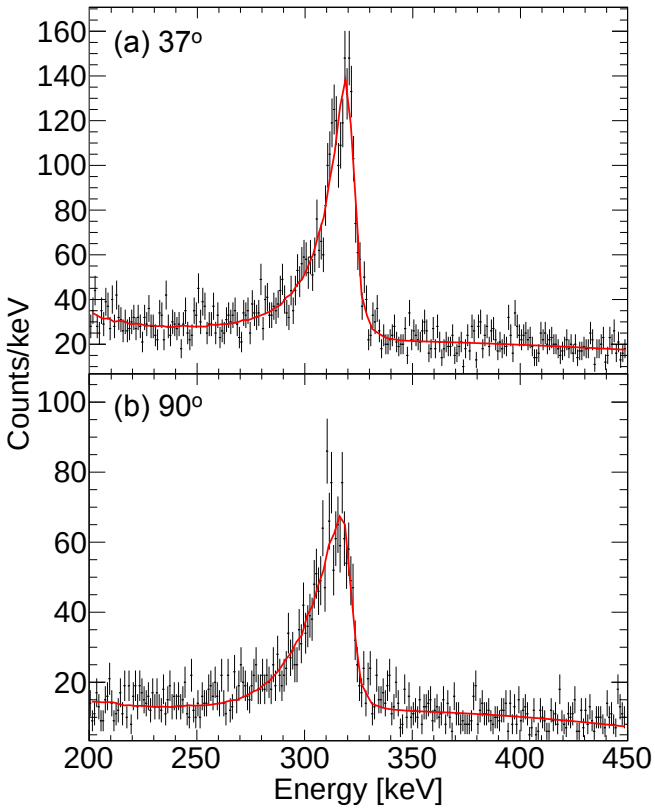

FIG. 4. (color online). The best-fit simulated line-shapes (red solid line) to the experimental data (black points), as determined using a reduced χ^2, for (a) the 37° SeGA ring data and (b) the 90° SeGA ring data of the 320(3) keV J^π:$(\frac{5}{2}^-_1)\rightarrow(\frac{7}{2}^-_{g.s})$ transition in ^{53}Ni.

tectors which in turn yields a broad, asymmetrical lineshape, with a centroid below the correct energy. This presents an opportunity for measurement of lifetimes, through a lineshape analysis, for the analogue transitions in this mirror pair. Half-lives were extracted through comparison of experimental γ-ray spectra with simulations generated using a dedicated lifetime code developed at NSCL [24] utilising the GEANT4 framework [25]. Although the simulation package also allows for the addition of feeding states, each of which have their own independent lifetimes and intensities, the lifetimes of the observed states feeding the $\frac{5}{2}^-_1$ state in ^{53}Mn are known to be small (<1 ps), and therefore were not included. It was assumed through mirror-symmetry arguments that these states were also short lived enough to be neglected for ^{53}Ni. A second-order polynomial background, which accurately replicated the experimental backgrounds in either the 37° and 90° SeGA rings, was added to the simulations over the region of lifetime sensitivity. The simulations were produced for both the 37° and 90° SeGA rings and fitted to the experimental spectra using a χ^2 minimisation method. For such an analysis, one of the required parameters to produce the simulated lineshape is the gamma-ray energy, which in the case of ^{53}Ni has not yet been accurately determined from the spectrum (the assumed value of 320(3)keV comes from the subtraction of the 1292(2) and 972(2) keV gamma-ray energies decaying from the $\frac{3}{2}^-_1$ state). Hence, in this analysis, both the gamma-ray energy and half-life were allowed to vary independently. This was done so that both the half-life and energy could be extracted for ^{53}Ni, and also so that the uncertainty in the gamma-ray energy could be accounted for in the result for the extracted half-life.

The resulting $\chi^2 - \chi^2_{min}$ plots for ^{53}Ni are shown in Fig. 3, where Fig. 3(a) shows the results for the simulated fits to the 37° experimental ring and Fig. 3(b) the 90° ring. It is clear that both the energy and half-life are well determined from this analysis, and also that the results for the two SeGA detector rings are consistent. Hence, it was possible to combine these results into a single $\chi^2-\chi^2_{min}$ plot, see Fig. 3(c), from which an energy of 320.5(2) keV and a half-life of 198(8) ps could be determined. These statistical errors come from the bounds, on each axis, of the $\pm1\sigma$ ellipse (solid line), which is derived from χ^2_{min}+1. In order to take account of the systematic errors in this analysis, we have assumed the the same systematic errors as Ref [24], in which lifetime measurements were performed for states with a very similar half-life and decay energy to those investigated in this work, and using an identical simulation code. The systematic error contributions included are: uncertainties due to ambiguities in the geometry of the setup (3%), γ-ray anisotropy effects (1.5%), assumptions in the background (3%) and finally effects due to feeding (1%), which in this case would include feeding of the $\frac{5}{2}^-_1$ state from short-lived states. (Although the geometrical arrangement of the gamma-ray detectors is slightly different in the two experiments, a similar systematic error is assumed.) Adding these uncertainties in quadrature results in an overall systematic error of 4.6%. Taking into account both the systematic and statistical error contributions, a half-life of 198(12) ps was determined for the $(\frac{5}{2}^-_1)$ state in ^{53}Ni. The lowest χ^2 fits to both the 37° and 90° SeGA ring data are also shown in Fig. 4. As a check, an identical approach was followed for the $\frac{5}{2}^-_1$ state in ^{53}Mn. However, in this case, the results for the simulated fits to the individual 37° and 90° SeGA rings were only consistent at the $\sim$2-σ level, yielding half-life measurements of 134(10) ps and 111(8) ps respectively. The discrepancy in these half-life measurements may have resulted due to uncertainties in the target position, which was estimated to be $\sim$3.5mm downstream of the center of the target chamber for this part of the experiment. In order to account for this, an additional systematic error of 11 ps (half the difference between the two independent half-life results) was included in the final error analysis for the weighted average result. This resulted in a weighted average half-life of 120(14) ps for the $\frac{5}{2}^-_1$ state in ^{53}Mn, which compares very favorably with the previous measurement of 117(6) ps [11].

Finally, we have measured, for both nuclei, relative

cross sections for knockout to the ground state and all the observed excited states – see Fig. 5(b) and (d). These were determined from the measured beam rate, using the efficiency-corrected γ-ray intensities, having subtracted observed feeding from higher-energy states. In this case, further corrections were made in ^{53}Mn by accounting for the intensities of previously-measured high-energy γ-rays (not observed due to low high-energy detection efficiency) decaying from the $(\frac{3}{2}^-_2)$ and $(\frac{5}{2}^+_1)$ states with known branching ratios. No such correction was made for ^{53}Ni, as this would require the uncertain assumption of equal branching ratios between the mirror pair.

IV. DISCUSSION

A. Knockout Cross Sections

Calculated, and estimated, relative cross sections are presented here for the one-neutron knockout from ^{54}Ni to ^{53}Ni. The purpose of this analysis is to understand the observed yields, give confidence to the deduced level schemes, and to investigate, more generally, the mirrored knockout process. The single-nucleon removal cross sections were calculated under the spectator-core approximation assuming eikonal reaction dynamics [26, 27]. The theoretical cross section for populating a specific residue state with spin-parity J^π is given by

$$\sigma_{th}(J^\pi) = \sum_{n\ell j} \left(\frac{A}{A-1}\right)^N C^2S\sigma_{sp}(n\ell j, S_N + E_x) \quad (2)$$

where C^2S is the shell model spectroscopic factor, $n\ell j$ denotes the quantum numbers of the nucleon removed and σ_{sp} is the single-particle cross section. The mass dependent term is the required centre-of-mass correction to the shell-model spectroscopic factors, with $N = 3$ for the fp-shell [28]. The single-nucleon wave functions were calculated in a Woods-Saxon potential (central plus spin-orbit), with diffuseness $a = 0.6$ fm and spin-orbit strength $V_{so} = 6$ MeV. The radius parameters r_0 of the binding potentials were constrained to reproduce the rms radii and binding energies of SkX interaction [29] Skyrme Hartree-Fock calculations. The depth of the central potential was then adjusted to give states at the appropriate effective separation energy S_N+E_x, where S_N is the projectile ground-state to residue ground-state nucleon separation energy and E_x the residue excitation. Densities, from the same Hartree-Fock calculations, were used in calculating the core-target S-matrices in the $t\rho\rho$ approximation (see, e.g., [30]). Spectroscopic factors were calculated using the ANTOINE code [31], using the KB3G [32] interaction in the full fp-shell space and therefore only population of negative parity states is calculated.

The calculated relative cross sections for ^{53}Ni and ^{53}Mn residues are shown in Figs. 5(a) and (c). In order to estimate the population of positive-parity states, resulting from one-nucleon knockout from the sd-shell,

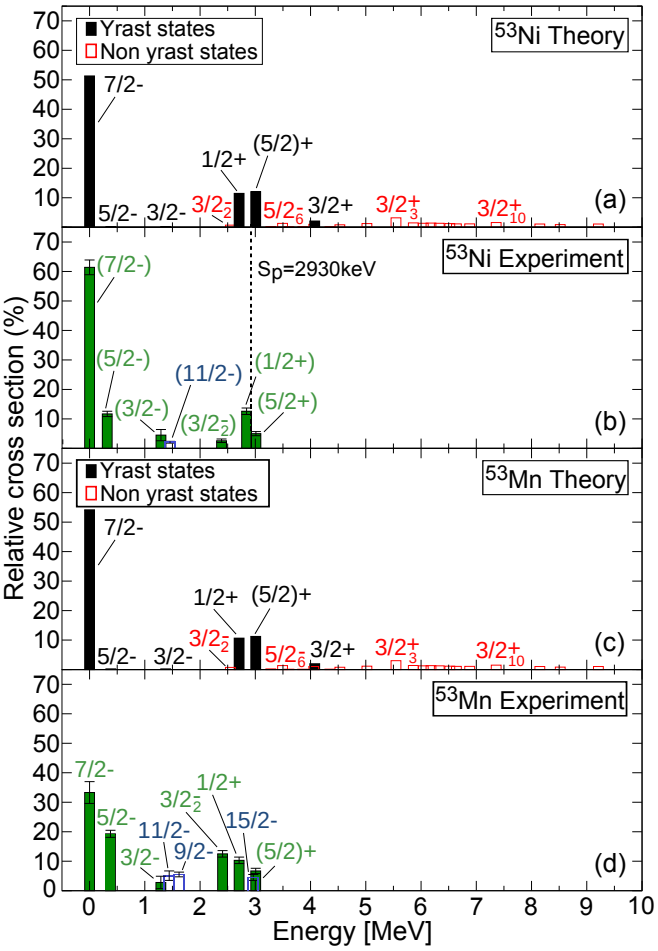

FIG. 5. (color online). Calculated and experimental relative cross sections for states in ^{53}Ni and ^{53}Mn, populated via one-neutron and one-proton knockout respectively. The calculations for ^{53}Ni and ^{53}Mn (panels (a) and (c)) were obtained using spectroscopic factors calculated in the shell-model, while spectroscopic factors for the positive parity states were taken from experimental data for ^{53}Mn and assumed to be the same for ^{53}Ni. The predicted relative cross sections and energies of both yrast states (black filled) and non yrast states (red unfilled) are shown. Panels (b) and (d) show the measured relative cross sections to states in ^{53}Ni and ^{53}Mn respectively, where statistical errors are also shown. States coloured in green (filled) can be compared with the calculated cross sections, while states coloured in blue (unfilled) can not be populated in direct knockout reactions from the ground state of the projectiles.

we have used previously extracted spectroscopic factors from transfer reactions onto ^{53}Mn [18], and assumed that these are the same for ^{53}Ni. Care needs to be taken with this approach since it is known [27, 33] that measured inclusive knockout cross sections are systematically smaller, by around a factor of 2 (for the separation energies concerned here), than cross sections calculated using theoretical spectroscopic factors from the shell model. Hence, a comparison of cross sections calculated using a

combination of theoretical and experimentally-deduced spectroscopic factors can only be used as a guide. Since the spectroscopic factors used for each member of the mirror pair are identical, the theoretical cross sections in panels (a) and (c) are virtually identical. Including positive parity states in the calculations in the way described previously, the majority of the intensity (∼50%) proceeds directly to the ground state, with ∼20% going to high-lying positive-parity states.

In order to compare these calculated cross sections with the experimental data, the other processes that may be present need to be considered. The maximum spin-parity state that can be populated in the direct, one-nucleon removal from ^{54}Fe or ^{54}Ni, with a ground state of 0^+, is $\frac{7}{2}^-$. However, states of higher-spin are observed in the two mirror nuclei. One possibility is that these high-spin states are populated in knockout reactions from high-spin isomeric states in both ^{54}Fe and ^{54}Ni. Indeed, a 10^+ spin-trap isomer has been previously observed in both ^{54}Fe and ^{54}Ni, with measured half-lives of 364(7) ns and 152(4) ns, respectively [34, 35]. Both of these isomers are sufficiently long-lived to still be present in the secondary beam at the secondary target position, after their initial population at the production target, since the ToF between these two targets is ∼300 ns.

One-nucleon knockout from these isomers could, in principle, populate a range of high-spin states from $\frac{13}{2}^-$ to $\frac{27}{2}^-$ in the final nuclei, and could explain in particular the observation of the $\frac{15}{2}^-$ and $\frac{13}{2}^-$ states in ^{53}Mn. Additional support for this argument comes from cross section calculations performed (using the same approach as described above) but assuming direct proton knockout from this isomer in ^{54}Fe to ^{53}Mn. Fig. 6 shows a theoretically-produced decay scheme, using experimental energies and branching ratios, assuming that these states are populated with the theoretically calculated cross sections. These calculations suggest that the entirety of the intensity from the strongly-populated states will feed through the $\frac{15}{2}^-$ and $\frac{13}{2}^-$ states and collect in the $\frac{11}{2}^-$ state. This may explain the strong γ-ray transition observed from this state, particularly in ^{53}Mn. This population of high-spin states does not appear to be mirrored in both daughter nuclei but instead appears to be much stronger in ^{53}Mn - see Fig. 2. This could be due to different initial isomeric ratios in the secondary beams, but will also be due, in part, to the shorter half-life of the ^{54}Ni 10^+ isomer, compared with that of ^{54}Fe. This will result in a smaller residual population of the isomer at the secondary target for knockout from ^{54}Ni to ^{53}Ni.

The theoretical and measured cross sections for ^{53}Ni are now compared – see Figs. 5(a) and (b). This reveals a fairly good level of agreement, although with a few differences. In particular, the $(\frac{5}{2})^+$ state appears to have a lower than predicted relative intensity by about a factor of two. However, the $(\frac{5}{2})^+$ analogue state in ^{53}Mn is known to have two other decay branches, which account for about half the decay strength, but which are not observed here due to their high decay energies. This has already been accounted for in ^{53}Mn in the $(\frac{5}{2})^+$ cross section measurement in Fig. 5(d). If a similar decay pattern exists in ^{53}Ni, then the measured $(\frac{5}{2})^+$ cross section in Fig. 5(b) is in reality a factor of two larger and would have a similar population intensity to that of the $(\frac{1}{2})^+$ state. However, we reiterate that since the spectroscopic factors for these states were taken from Ref. [18] rather than shell model calculations, their branches should only be considered as a guide. Fig. 5(b) also shows population of a number of other low-lying states in ^{53}Ni, with a much higher relative cross section than expected, see for example $(\frac{5}{2}{}_1^-)$, $(\frac{3}{2}{}_1^-)$ and $(\frac{3}{2}{}_2^-)$. It is probable that these states are populated via fast E1 transitions from a number of low-spin, high-energy, positive-parity states which are expected to be populated (see Fig. 5(a)), with a combined total relative cross section of ∼20%. Indeed, in ^{53}Mn, several such decay paths are known to exist. This, and decays from other high-lying negative parity states, will contribute to the observed low-lying negative parity strength. In general, and especially having considered these additional decay-branching issues, the agreement between both Fig. 5(a) and (b), and Fig. 5(c) and (d), is reasonable.

Finally, we compare the experimental relative cross section distributions for the mirror pair - see Fig. 5(b) and (d). One would intuitively expect these to be identical, given the mirrored reaction process, but some differences are apparent - e.g. the $\frac{3}{2}{}_2^-$ and $\frac{5}{2}{}_1^-$ states, and the different relative population of the ground states. Firstly, as has been discussed earlier, there is strong evidence for the presence of the 10^+ isomers in the beams - with a much stronger residual population of the isomer at the secondary target for ^{54}Fe. This accounts for the additional intensity for $\frac{9}{2}^-$, $\frac{11}{2}^-$ and $\frac{15}{2}^-$ in ^{53}Mn. It has also been pointed out earlier that some higher-lying low-spin states are expected to be populated in both nuclei, and could cascade through the low-lying states - such as the $\frac{3}{2}{}_2^-$ and $\frac{5}{2}{}_1^-$ states. In ^{53}Ni some of these high-energy states will also be proton unbound (S_p = 2930 keV [36]) and these could decay by proton emission rather than gamma decay. In the analysis presented here, the effect would be to artificially increase the ground-state experimental cross section of ^{53}Ni. This effect also needs to be considered when comparing the experimental and theoretical cross sections for ^{53}Ni – Figs. 5(a) and (c). Finally, the data seems to indicate that the transition observed from the $\frac{3}{2}{}_2^-$ state in ^{53}Mn is a doublet, and that this has artificially inflated the relative cross section to that state of ^{53}Mn in Fig. 5(d), and hence artifically reduced the apparent cross section to the ground state. In this analysis, it should also be noted that any high-lying states populated, which directly feed the ground state, will also lead to an overestimation of the relative cross section to the ground state, and such effects may be slightly different between the mirror nuclei.

The conclusion from this analysis is that the relative

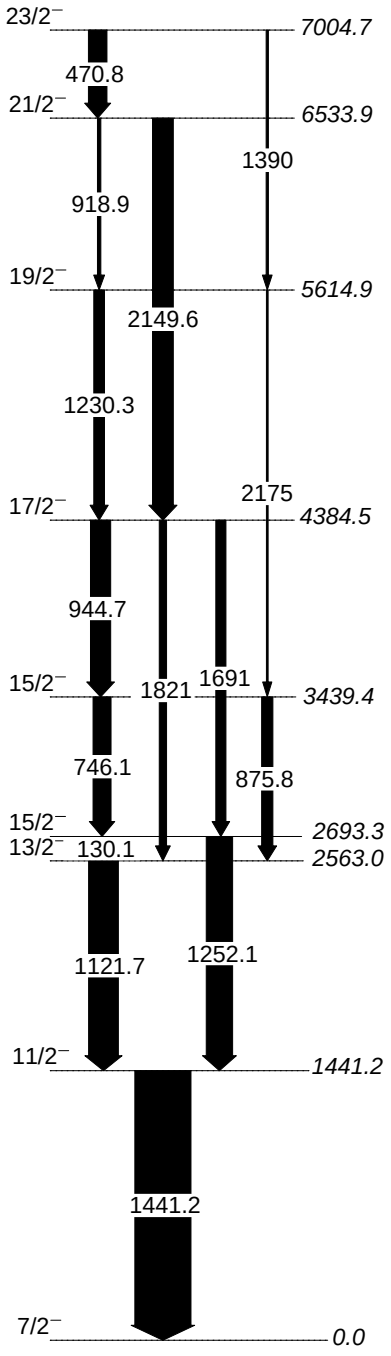

FIG. 6. An energy level scheme of ^{53}Mn showing the states strongly populated in one-proton knockout from the ^{54}Fe 10^+ spin-trap isomer. The population of each state is predicted from cross section calculations using the method described in the text, with spectroscopic factors calculated using the ANTOINE code [31] in the full fp valence space using the KB3G interaction [32]. Information on the state energies and branching ratios were used from previous experimental studies on ^{53}Mn [10].

population of the states in both nuclei can be understood well in terms of the direct knockout processes, assuming symmetry between the spectroscopic factors of the mirror pair and having accounted for the presence of isomeric states in the beams. This again gives confidence in the assignments made for the newly identified states in ^{53}Ni.

B. Mirror Energy Differences

Having established the level scheme for ^{53}Ni, the experimental MEDs for the ^{53}Ni/^{53}Mn pair can be extracted – these are shown in Fig. 7(a). The work presented here has confirmed the data points at $\frac{5}{2}^-$ and $\frac{11}{2}^-$ observed by Brown *et. al.* [8] and added the two data points at $\frac{3}{2}^-$. In order to interpret these data, large-scale shell-model calculations, using the ANTOINE code [31], were performed for the ^{53}Ni/^{53}Mn mirror pair, using the full fp valence space and the KB3G interaction [32]. No restrictions were placed on the movement of particles between the fp orbitals. Adopting an identical approach to that described in Ref. [4], four isospin-breaking components, and their subsequent contribution to the MED, were then calculated. These four terms are as follows: (a) The V_{CM} term which accounts for the multipole Coulomb interaction by the addition of Coulomb matrix elements to the effective two-body interaction for protons. (b) The radial term (V_{Cr}) is a monopole term which accounts for the Coulomb energy associated with changes in mean nuclear radius, in accordance with [6]. (c) The V_{ll} and V_{ls} terms account for Coulomb [6] and electromagnetic spin-orbit shifts [37] of the single particle levels. (d) The V_B term represents an additional isovector term for the $J = 2$ channel, included by adding an additional repulsive term of 100 keV for $f_{\frac{7}{2}}$ protons at $J = 2$. It has been found, empirically, to be necessary to include this correction term to achieve reasonable agreement with the data [4, 6]. Since the monopole terms, generally, have a dependence on T_z, the effects of V_{Cr}, V_{ll} and V_{ls} may become enhanced with increasing difference in proton number between the mirror nuclei. This work provides a good test of this shell-model prescription and builds upon previous work [3, 8], already showing excellent agreement at large isospin of $T_z = \pm 2$ and $T_z = \pm\frac{3}{2}$.

The results of the shell-model calculations are shown in Fig. 7(a). As already suggested by Brown *et al.* [8], the inclusion of the isospin non-conserving (V_B) term, shown by the dotted line in Fig. 7(a), results in an improvement in the fit to the experimental data, compared to the dashed line, where no V_B term has been included. This is consistent with the recent findings in this region – e.g. references [3, 4, 8] – which have indicated that inclusion of this V_B term for just $J = 2$ $f_{\frac{7}{2}}$ matrix elements provides, broadly, a better description of experimental MED. However, rather than using a single isospin non-conserving matrix element, a recent study [7] has extracted a full set of effective isovector ($pp - nn$) matrix elements in the $f_{\frac{7}{2}}$ shell by fitting the shell model to all experimental MED data so far obtained in the shell. This has yielded matrix elements of $V_B = -72, +32, +8, -12$ keV

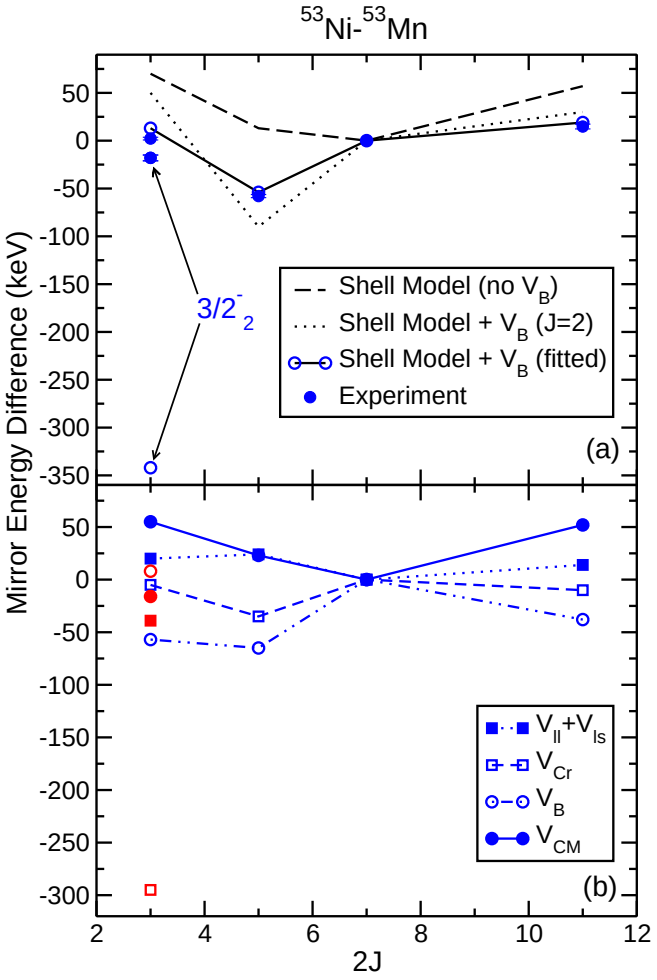

FIG. 7. (color online) (a) A comparison between the experimental MED and the shell-model calculations. The dotted line shows the shell-model calculations including the V_B term for $J = 2$ only, the solid line shows inclusion of the fitted parameters for V_B, and the dashed line shows the calculations with no V_B term included – see text for details. Data for both $\frac{3}{2}^-$ states are included, and the lines only connect the yrast states. (b) The four isospin-breaking components of the shell-model calculations (described within the text), the sum of which yields the solid line in (a). For the V_B term, the fitted parameters have been used – see text for details. The theoretical data points for yrast states and non-yrast states are colored blue and red, respectively, where the lines only connect the yrast states.

for $J = 0, 2, 4, 6$ couplings of the $f_{\frac{7}{2}}$ orbital (note again the rise of about 100 keV from $J = 0$ to $J = 2$). The results of a shell-model calculation, performed when these four matrix elements are added to the two-body interaction for protons, is shown by the solid line in Fig. 7(a). There is an obvious further improvement in the agreement, which is now excellent. It should be noted that the three excited states presented in this work (the $\frac{3}{2}^-_1$, $\frac{5}{2}^-$ and $\frac{11}{2}^-$ states) are included in the fit, which is made up from 93 pairs of excited states in 17 mirror nuclei between $A = 42$ and 54. Exclusion of these states from the fit changes the result by less than 1 keV. The four components of the shell-model calculation, as described above, are shown in Fig. 7(b), where the fitted values of $V_B = -72, +32, +8, -12$ keV [7] are used.

It is clear from Fig. 7(a) that a significant discrepancy appears for the non-yrast $\frac{3}{2}^-_2$ state, and an inspection of the various components of the MED in Fig. 7(b) indicates that this is due to the V_{Cr} term. The V_{Cr} term is intended [6] to track changes in radii along the yrast band, and determine the resulting MED contribution due to the difference in proton number. In the model, the $p_{\frac{3}{2}}$ occupancy is tracked to determine the size of the effect [6]. However, the wavefunction of the $\frac{3}{2}^-_2$ state contains a significant fraction of a pure $p_{\frac{3}{2}}$ single-particle configuration, unlike the rest of the states considered. This suggests that this method for calculating the V_{Cr} term may not be appropriate when pure single-particle excitations of this kind are present.

C. Half-life of the $\frac{5}{2}^-_1$ state

In this work, the half-life of the $\frac{5}{2}^-_1$ state in ^{53}Ni (198(12) ps) was established, allowing a high-precision comparison with its mirror ^{53}Mn (117(6) ps [11]). The γ-ray transition from the state in ^{53}Mn is known to be highly mixed E2/M1 ($|\delta| = 0.61(8)$ [38]). It is not possible with the current data to determine a mixing ratio for the transition in ^{53}Ni, and so no absolute values of the $B(M1)$ or $B(E2)$ can be extracted for ^{53}Ni. However, the data do still constrain the relative values of the $B(E2)$s and $B(M1)$s as indicated in Figure 8. In the figure, the value of the unknown mixing ratio δ^2_{Ni} is allowed to vary freely between 0 and 1, and the experimental data for the γ-ray energies, lifetimes and the known value of δ^2_{Mn} are then used to calculate, and plot, $\frac{B(E2)_{Ni}}{B(E2)_{Mn}}$ *vs.* $\frac{B(M1)_{Ni}}{B(M1)_{Mn}}$ – see the solid diagonal line. The dashed lines indicate the error bounds resulting from the errors in δ^2_{Mn}, the γ-ray energy (in ^{53}Ni) and the two half-lives. The region consistent with the experimental data, within error, is therefore between the dashed lines. The range of $0 \leq \delta^2_{Ni} \leq 1$ does not contain the full range of possibilities, but was chosen as it is this range that contains the region of similar transition strengths between the mirrors and is the region close to the shell-model prodictions. Using the full range of possible δ^2_{Ni} values extends the plot to the upper left towards $(x, y) = (0, \sim 5)$.

Considering the $B(E2)$s initially, if we assume perfect symmetry in the analogue wavefunctions of the states concerned, then intuitively one might expect the $B(E2)$ in ^{53}Ni to be reduced compared with its mirror. This is because the number of active valence protons should be very different: ^{53}Ni will have an (approximately) closed shell of protons, and ^{53}Mn an (approximately) closed shell of neutrons. The large difference in T_z in this case should then result in a reduction in $B(E2)$ for ^{53}Ni com-

pared with ^{53}Mn. The data indicates that if this were the case in reality, then the ratio $\frac{B(M1)_{Ni}}{B(M1)_{Mn}}$ should be ≥ 1 - i.e. the $B(M1)$ would be larger for ^{53}Ni.

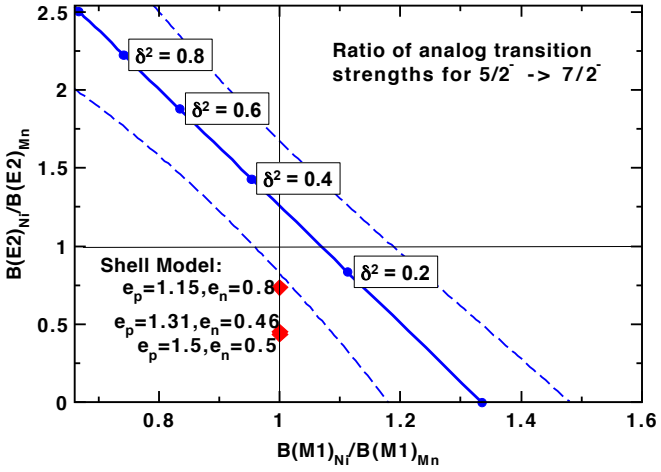

FIG. 8. (color online) Data corresponding to the transition between the $\frac{5}{2}^-$ first-excited state and ground state in both members of the A=53 mirror pair. The ratio of the analogue $B(E2)$s is plotted as a function of the ratio of the analogue $B(M1)$s. The $E2/M1$ mixing ratio is unknown for the ^{53}Ni transition, and so the solid line represents the range of data corresponding to values of δ^2 from 0 to 1. This range of values was chosen as it correspond to the region of the theoretically calculated data points. The dashed lines represent the experimental limits. The red points mark the predictions of the shell-model based on the data in Table I.

The $B(M1)$ and $B(E2)$ transition strengths have been calculated in the shell model for both members of the mirror pair, and the results are summarised in Table I. The calculations have been performed using the full set of isospin-breaking terms as described above, and use effective g-factors and three different sets of effective charges. The first are the effective charges from du Rietz *et al.*, $\epsilon_p = 1.15, \epsilon_n = 0.8$, derived from mirror nuclei in the upper $f_{\frac{7}{2}}$ shell [39]; the second are the effective charges from Dufour and Zuker [40]; the third are the "standard" shell-model effective charges of $\epsilon_p = 1.5, \epsilon_n = 0.5$. Since we are effectively swapping neutron holes for proton holes in this mirror pair, the difference in the $B(E2)$ should be very sensitive to the effective charges chosen in the shell model – and the table confirms this to be the case.

The shell-model over-predicts the half-life of both states significantly in all the calculations, due to the underestimation of the $B(M1)$ strength - as can be seen from the measured $B(M1)$ in ^{53}Mn. In considering the relative values of the $B(E2)$s and $B(M1)$s between the mirrors, the three sets of shell-model calculations are indicated in Figure 8. The shell-model, as expected, predicts that the $B(E2)$ for ^{53}Ni is indeed significantly lower than for ^{53}Mn. It is noteworthy that the effective charges from du Rietz *et al.*, $\epsilon_p = 1.15, \epsilon_n = 0.8$, extracted from the neighboring A=51 $T_z = \pm\frac{1}{2}$ mirror pair, yield a set

	^{53}Mn	^{53}Ni
Experiment		
$T_{1/2}$ (ps)	117(6) [11]	198(12)
$B(M1)^a$ (μ_N^2)	0.0045(4)	-
$B(E2)^a$ (e^2fm^4)	159(34)	-
Shell Model: $\epsilon_p = 1.15, \epsilon_n = 0.8$ [39]		
$T_{1/2}$ (ps)	232	551
$B(M1)$ (μ_N^2)	0.0011	0.0011
$B(E2)$ (e^2fm^4)	204	150
Shell Model: $\epsilon_p = 1.31, \epsilon_n = 0.46$ [40]		
$T_{1/2}$ (ps)	231	678
$B(M1)$ (μ_N^2)	0.0011	0.0011
$B(E2)$ (e^2fm^4)	206.1	92.7
Shell Model: $\epsilon_p = 1.5, \epsilon_n = 0.5$		
$T_{1/2}$ (ps)	194	620
$B(M1)$ (μ_N^2)	0.0011	0.0011
$B(E2)$ (e^2fm^4)	267	116

TABLE I. Comparison of the experimental and theoretical half-lives, $B(E2)$s and $B(M1)$s for the analogue transitions between the $\frac{5}{2}^-$ first-excited state and ground state in the A=53 mirror pair. The $M1/E2$ mixing ratio is unknown for the ^{53}Ni transition, and so the individual $B(E2)$ and $B(M1)$ are undetermined. Theoretical predictions come from the shell-model predictions using three sets of effective charges, including those of du Rietz *et al.* [39] and Dufour and Zuker [40]. The $B(M1)$s are calculated using effective g-factors ($g_l^{eff} = g_l^{free} \pm 0.1$, with ± 0.1 for p,n respectively, and $g_s^{eff} = 0.75 g_s^{free}$). The shell model half-lives were calculated using experimental energies.

[a] *The individual $B(M1)$ and $B(E2)$ for ^{53}Mn have been determined using the published mixing ratio of $|\delta| = 0.61(8)$ [38].*

of predictions that lie closer to the experimental data. The shell-model under-predicts the $B(M1)$s significantly, although they are very weak and hence a detailed comparison with the model is not appropriate. Information on the E2/M1 mixing ratio for ^{53}Ni is clearly needed in order to make a more complete analysis.

V. CONCLUSION

In conclusion, new states and γ-ray transitions have been identified in the proton rich nucleus ^{53}Ni ($T_z = -\frac{3}{2}$). A new level scheme has been constructed, using arguments based on mirror symmetry (both of the schemes and of the knockout process) and a γ-γ coincidence analysis. The observation of mirrored hole states, based on excitations from $d_{\frac{5}{2}}$ (though possibly $d_{\frac{3}{2}}$) and $s_{\frac{1}{2}}$, is presented. MED have been computed and compared to large-scale shell-model calculations. These are interpreted in terms of isospin non-conserving effects, demonstrating an improvement in the fit to the data due to the inclusion of a set of isovector isospin-non-conserving matrix elements – in addition to the Coulomb term – which have a strong $J-$dependence. Detailed comparisons have been made between experimental and theoretical relative

cross sections for one-nucleon knockout reactions leading to the mirror pair. A high degree of symmetry is observed in the knockout process, with differences discussed in terms of binding-energy effects and the presence of isomers in the secondary beams. A reasonable agreement with the theoretical cross sections is obtained. Finally, a comparison of mirrored lifetimes has been made possible by measurement of the long-lived $\frac{5}{2}^-$ yrast state in ^{53}Ni using lineshape analysis, resulting in a half-life measurement of 198(12) ps.

This work was supported by the UK Science and Technology Facilities Council (STFC) under Grants No. ST/J000124, No. J000051, and No. J000132, and the National Science Foundation (NSF) under Grant No. PHY-1102511.

[1] E. Wigner, Phys. Rev. 51, **106** (1937).
[2] R. Machleidt and I. Slaus, J. Phys. G: Nucl. Part. Phys. **27**, R69 (2001).
[3] P.J. Davies *et al.*, Phys Rev Lett. **111**, 072501 (2013).
[4] M.A. Bentley and S.M. Lenzi, Prog. Part. Nucl. Phys. **59**, 497 (2007).
[5] J. Ekman, C. Fahlander and D. Rudolph, Mod. Phys. Lett. **A20**, 2977 (2005).
[6] A. P. Zuker, S.M. Lenzi, G. Martínez-Pinedo, and A.Poves, Phys. Rev. Lett. **89**, 142502 (2002).
[7] M.A. Bentley, S.M. Lenzi, S.A. Simpson and C.Aa. Diget, Phys Rev C **92** 024310 (2015).
[8] J.R. Brown *et al.*, Phys. Rev. C **80**, 011306 (2009).
[9] P. Fintz *et al.*, J.Phys. (Paris) **40**, 511 (1979).
[10] H. Junde, Nuclear Data Sheets **110** 2689 (2009).
[11] S. Gorodetzky *et al.*, Nuclear Physics **85**, 519 (1966).
[12] M.A. Bentley *et al.*, Modern Physics Letters A, **25**, 21-23 (2010).
[13] D.J. Morrissey, B.M. Sherrill, M. Steiner, A. Stolz, and I. Wiedenhoever, Nucl. Instrum. Methods Phys. Res., Sect. B **204**, 90 (2003).
[14] D.J. Morrissey, Nucl. Instrum. Methods Phys. Res., Sect. B **126**, 316 (1997).
[15] D. Bazin, J.A. Caggiano, B.M. Sherrill, J. Yurkon, and A. Zeller, Nucl. Instrum. Methods Phys. Res., Sect. B **204**, 629 (2003).
[16] J. Yurkon, D. Bazin, W. Benenson, D.J. Morrissey, B.M. Sherrill, D. Swan, and R. Swanson, Nucl. Instrum. Methods Phys. Res., Sect. A **422**, 291 (1999).
[17] W.F. Mueller, J.A. Church, T. Glasmacher, D. Gutknecht, G. Hackman, P.G. Hansen, Z.Hu, K.L. Miller, and P. Quirin, Nucl. Instrum. Methods Phys. Res., Sect. A **466**, 492 (2001).
[18] N.G. Puttaswamy *et al.*, Nuclear Physics A **401**, 2 (1983).
[19] E. Newman and J.C. Hiebert, Nuclear Physics A **110** 366 (1968)
[20] P.D. Georgopulos, E.J. Hoffman and D.M. Van Patter. Nuclear Physics **226**, 1 (1974).
[21] O.B. Tarasov and D. Bazin, Nucl. Instrum. Methods Phys. Res., Sect. B, **266**, 19-20 (2008).
[22] R.L. Schulte, J.D. King, H.W. Taylor, Nuclear Physics A **243**, 2 (1975).
[23] P.M. Endt, Atomic Data and Nuclear Data Tables, **23**, 6 (1979).
[24] A. Lemasson, *et al.*, Phys. Rev. C **85**, 041303 (2012).
[25] S. Agostinelli, *et al.*, Nucl. Instrum. Methods Phys. Res. Sect. A **598**, 250303 (2003).
[26] P.G. Hansen and J.A. Tostevin, Ann. Rev. Nucl. Part. Sci. **53**, 219 (2003).
[27] A. Gade *et al.*, Phys. Rev. C **77**, 044306 (2008).
[28] A. E. L. Dieperink and T. de Forest, Phys. Rev. C 10, 543 (1974).
[29] B.A. Brown, Phys. Rev. C **58**, 220 (1998).
[30] J.S. Al-Khalili and J.A. Tostevin, Phys. Rev. Lett. **76**, 3903 (1996).
[31] E. Caurier and F. Nowacki, Acta Phys. Pol. B **30** 705 (1999).
[32] A. Poves, J. Sanchez-Solano, E. Caurier and F. Nowacki, Nucl. Phys. A **694**, 157 (2001).
[33] J. A. Tostevin and A. Gade, Phys. Rev. C **90**, 057602 (2014).
[34] E. Dafni *et al.*, Phys. Lett. B **76**, 1, 50-53 (1978).
[35] D. Rudolph *et al.*, Phys. Rev. C **78**, 021301 (2008).
[36] M. Wang, G. Audi, A.H. Wapstra, F.G. Kondev, M. MacCormick, X. Xu and B. Pfeiffer, Chin.Phys.C **36**, 1603 (2012).
[37] J.A. Nolen and J.P. Schiffer, Annu. Rev. Nucl. Sci. **19**, 471 (1969).
[38] P.H. Vuister, Nuclear Physics A **91**, 521 (1967).
[39] R. du Rietz *et. al.*, Phys. Rev. Lett. **93**, 222501 (2004)
[40] M. Dufour and A.P. Zuker, Phys. Rev. C **54**, 1641 (1996).